Multi-temporal monitoring of wheat growth by using images from satellite and unmanned aerial vehicle

Du Mengmeng[1], Noguchi Noboru[2*], Itoh Atsushi[3], Shibuya Yukinori[3]

(1. *Graduate School of Agriculture, Hokkaido University, Sapporo 065-8589, Hokkaido, Japan*;
2. *Research Faculty of Agriculture, Hokkaido University, Sapporo 065-8589, Hokkaido, Japan*;
3. *Hokkaido Agricultural Research Center, Memuro 082-0081, Hokkaido, Japan*)

Abstract: Recently near-ground remote sensing using unmanned aerial vehicles (UAV) witnessed wide applications in obtaining field information. In this research, four Rapideye satellite images and eight RGB images acquired from UAV were used from early June to the end of July, 2015 covering two experimental winter wheat fields, in order to monitor wheat canopy growth status and analyze the correlation among satellite images based normalized difference vegetation index (NDVI) with UAV's RGB images based visible-band difference vegetation index (VDVI) and ground variables of the sampled grain protein contents. Firstly, through image interpretation of UAV's multi-temporal RGB images with fine spatial resolution, the wheat canopy color changes could be intuitively and clearly monitored. Subsequently, by monitoring the changes of satellite images based NDVI as well as VDVI values and UAV's RGB images based VDVI values, the conclusions were made that these three vegetation indices demonstrated the same and synchronized trend of increasing at the early stage of wheat growth season, reaching up to peak values at the same timing, and starting to decrease since then. The results of the correlation analysis between NDVI of satellite images and sampled grain protein contents show that NDVI has good predicative capability for mapping grain protein content before ripening growth stage around June7, 2015, while the reliability of using satellite image based NDVI to predict grain protein contents becomes worse as ripening stage approaches. The regression analysis between UAV's RGB image based VDVI and satellite image based VDVI as well as NDVI showed good coefficients of determination. It is concluded that it is feasible and practical to temporally complement satellite remote sensing by using UAV's RGB images based vegetation indices to monitor wheat growth status and to map within-field spatial variations of grain protein contents for small scale farmlands.

Keywords: satellite remote sensing, UAV remote sensing, wheat growth monitoring, wheat lodging; wheat protein content, multi-temporal images, NDVI
DOI: 10.25165/j.ijabe.20171005.3180

Citation: Du M M, Noguchi N, Itoh A, Shibuya Y. Multi-temporal monitoring of wheat growth by using images from satellite and unmanned aerial vehicle. Int J Agric & Biol Eng, 2017; 10(5): 1–13.

1 Introduction

Agronomic management in accordance with growth status during each wheat development stage is critical to optimize wheat yield and grain quality. According to Zadoks Code, wheat growth stages are generally divided into 10 distinct development stages including emergence stage, tillering stage, booting stage, heading stage, flowering stage, dough development stage, and ripening stage etc.[1], and necessary field operations such as different rates of nitrogenous topdressing should be implemented timely. Furthermore, recent studies on canopy management showed that not only topdressing rate but timing also should be tailored to achieve desired canopy sizes for specific development phases to optimize inputs and yield[2]. Therefore, real time monitoring of

Received date: 2017-01-07 **Accepted date:** 2017-06-12
Biographies: Du Mengmeng, PhD candidate, research interests: precision agriculture, image processing, Email: dumm@bpe.agr.hokudai.ac.jp; **Itoh Atsushi**, PhD, Senior Researcher, research interests: information and communication technology in farming system, Email: aitoh@affrc.go.jp; **Shibuya Yukinori**, Senior Researcher, research interests: information and communication technology in farming system, Email: yukky@affrc.go.jp.
***Corresponding author: Noguchi Noboru**, PhD, Professor, research interests: vehicle robotics, precision agriculture. Research Faculty of Agriculture, Hokkaido University, Kita 9 Nishi 9, Sapporo 065-8589, Hokkaido, Japan, Tel: +81-11-706-3847. Email: noguchi@cen.agr.hokudai.ac.jp.

actual wheat canopy's growth status is of great importance during wheat growing season.

Traditionally, in order to understand canopy development status during tillering stage, wheat tillers within unit area are manually counted by randomly taking samples around the investigated farmland so that general information of tiller density could be grasped and accordingly different timings and rates of nitrogenous fertilizing could be determined for each specific farmland[3]. On the other hand, agricultural remote sensing has been successfully used as an effective alternative for obtaining field information by using various kinds of vegetation indices calculated from the reflectance or radiance of specific bands. Normalized difference vegetation index[4], known as NDVI, is one of the most popular indicators to identify vegetated areas, estimate crop yields, and even to quantify the photosynthetic capacity of plant canopies since 1970s[4,5] On the basis of different types of platforms that carry specific sensors, agricultural remote sensing could generally be categorized into satellite remote sensing, airborne remote sensing, and near-ground remote sensing. Agricultural satellite imagery generally collects reflectance of solar illuminance, which is usually categorized as passive remote sensing[6]. RapidEye satellites built by MacDonald Dettwiler, Ltd were launched from August 29th, 2008[7], which provides frequent global revisit intervals of one day. Identical push-broom sensors carried on each satellite collect multispectral data of five spectral bands including blue (440-510 nm), green (520-590 nm), red (630-685 nm), red edge (690-730 nm), and near-infrared (760-850 nm) with 77 km swath width. During on-ground processing the remote sensing imagery is radiometrically calibrated and scaled to a 16 bit dynamic range, which converts the relative pixel digitized number into values related with at sensor radiances by a radiometric scale factor of 0.01[8]. High spatial resolution of 6.5 m of level 1B products and 5 m in terms of nadir ground sampling distance of the ortho-rectified ones is the another merit in consideration of the study on combination of satellite remote sensing images based vegetation indices with UAV's RGB images based vegetation indices. However, high cost, low spatial resolution, as well as atmospheric effects or weather interference of satellite images is known as the inherent flaws in precision agriculture domain. Therefore, airborne remote sensing has been introduced into medium-scale agricultural applications as a supplementary method of satellite remote sensing. Airplanes or balloons are usually used as sensor carriers, flying at the height of from less than 5000 m to 20 000 m, and spatial resolution of digital photography could reach up to 1 m[9]. Near-ground remote sensing is often referred to cutting edge application of small fixed-and/or rotary-wing unmanned aerial vehicles (UAVs) used in small-scale and experimental field for spatial sampling or mapping for variable-rate operations[10]. UAVs' payload varies from several hundred grams to dozens of kilograms, with various kinds of commercial cameras, multi-spectral cameras, and laser rangers mounted upon[11].

In recent years, civilian applications of small-UAVs have been widespread from entertainment industry to professional photogrammetry, hazard survey, crop protection, agricultural remote sensing, etc., as UAV's RGB imagery has increasing spatial resolution, may be acquired more cost-effectively and with excellent maneuverability as well as greater safety when compared with manned aircrafts[12]. Besides, agricultural application of UAV remote sensing by using commercial color cameras provides instantly researchers and farmers with actual and intuitive visualization of crop growth status, since color images accentuate particular vegetation greenness and have been suggested to be less sensitive to variations of illumination conditions[13,14]. Meanwhile the application of commercial color cameras also decreases the high cost of remote sensing sharply, since most digital cameras use a Bayer-pattern array of filters to obtain a RGB image and acquisition of near-infrared band often requires an extra filter which converts digital numbers of either blue or red light in Bayer array into near-infrared readings through massive post-processing and calibration work[15]. Furthermore, several vegetation indices based on color images were proposed

such as visible-band difference vegetation index (VDVI)[14], among other color vegetation indices of normalized green-red difference index (NGRDI)[16], normalized green-blue difference index (NGBDI)[12], and green-red ratio index (GRRI)[16], and excessive greenness (ExG)[18]. Wang et al.[14] distinguished vegetative areas from non-vegetative areas by analyzing color images acquired from a UAV and found VDVI has the most precise capability of extracting vegetation areas in comparison with other vegetation indices of NGRDI, NGBDI, GRRI, and ExG. Rasmussen et al.[19] investigated four different vegetation indices acquired from a color camera and a color-infrared camera by using both a fixed-wing and a rotary-wing UAV, and concluded that vegetation indices based on UAV's RGB image have the same ability to quantify crop responses with ground-based recordings. In our last research paper[12], we reported wheat yield correlated with four accumulative color vegetation indices of visible-band difference vegetation index (VDVI), normalized green-blue difference index (NGBDI), green-red ratio index (GRRI), and excess green vegetation index (ExG) by using stepwise regression method, with good coefficient of determination and RMSE as 0.94 and 0.02. Therefore, in this study we investigated the correlations between vegetation indices of UAV's RGB images and satellite images in order to temporally complement satellite remote sensing by using images of UAV remote sensing system. Vegetation indices from different sources were also used to conduct correlation analysis with the sampled grain protein contents for mapping within-field variations of grain protein contents.

2 Materials and methods

In this research, four Rapideye satellite images were used to conduct correlation analysis between satellite images based NDVI and ground variables of grain protein contents. The satellite images were taken on June 1, 7, 15, and July 17, 2015 over the vicinity of 42°54'10"N and 142°53'57"E in Hokkaido, Japan. Since satellite remote sensing images' temporal frequencies and spatial resolution are not adequate to monitor rapidly changing wheat growth conditions, eight RGB images acquired from UAV were also taken from early June to the end of July 2015 covering two experimental wheat fields at interval of about one week. As the result, the most relevant growth stage that affects the differentiation of grain protein contents could be determined. Based on the temporally complementary satellite images and UAV's RGB images, the authors of this paper also analyzed the correlations among satellite remote sensing images based vegetation indices and UAV's RGB image based vegetation index, to discuss the feasibility of utilizing UAV's RGB images to temporarily complement satellite remote sensing in case that satellite images were not available or cost-efficient over specific areas. Finally, through visual inspection of UAV's RGB images, occurrence of crop lodging was notified, which could be used to guide drivers or autonomous harvesting vehicles to adjust operation speed according to specific lodging situations for less harvesting loss.

2.1 Field site

Experiments were established on two neighboring fields, which were planted with two different winter wheat varieties of Kitahonami and Yumechikara around September 25, 2014 and harvested on July 27, 2015. Figure 1 showed the location of the investigated farmland in Memuro, Hokkaido, Japan. From weather data of 1981-2015[20], regional annual precipitation, average annual temperature, and average accumulative annual duration of sunshine of this area is reported as 953.3 mm, 6.2°C, and 1939.6 h, respectively, while in 2015 annual precipitation, average annual temperature, and accumulative annual duration of sunshine of this area is reported as 828.5 mm, 7.0°C, and 2115.0 h, respectively. The lower left field No.1 (marked in black rectangle shown in Figure 2) and upper right field No.2 (marked in red rectangle shown in Figure 2) was planted with wheat variety of Kitahonami and Yumechikara, respectively. Each of these two fields occupies about 3.3 hm^2 and 2.2 hm^2, of which the variety of Kitahonami is the most widely planted winter wheat variety in Japan and is reported to have taken up about 90% acreages of winter wheat in Hokkaido alone[21].

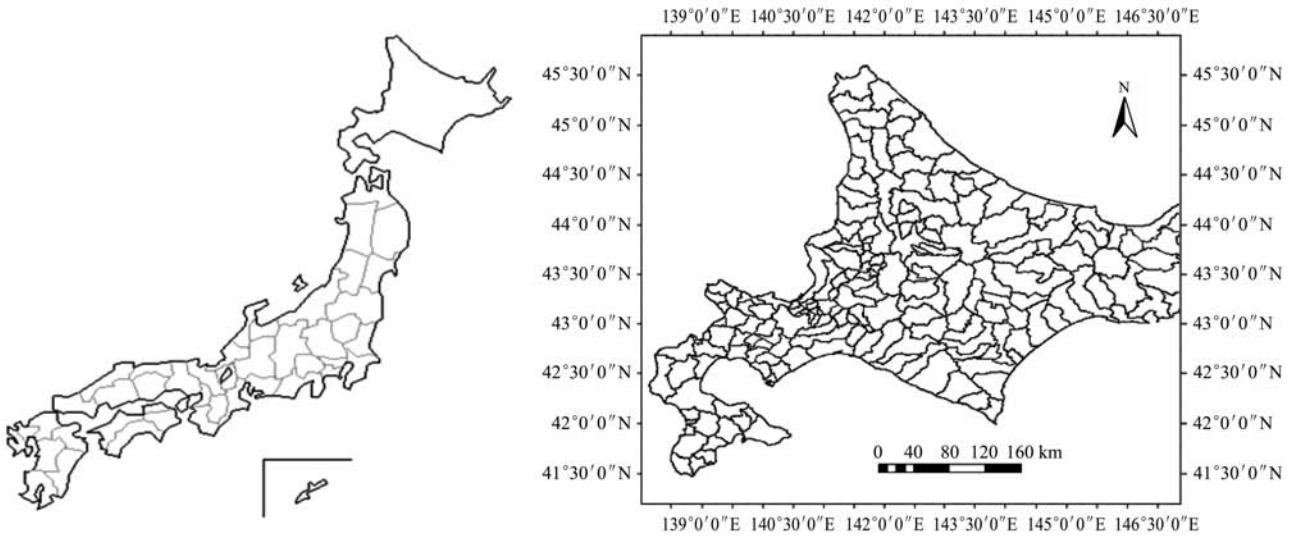

Figure 1 Field site of the farmland under investigation

Figure 2 Two neighboring wheat fields were studied planted with different winter wheat varieties

Table 1 UAV flight plan and camera specifications

Flying altitude/m	100
Ground speed/km·h^{-1}	2
Duration of flight/min	9
Flight date (around 11:00 at local time)	June 2, 10, 19, 25; July 2, 10, 16, 24, 2015.
Camera resolution/pixels	4000×6000
Sensor size/mm	23.5×15.6

Figure 3 Quadrotor was used as platform of UAV-camera system

2.2 UAV's RGB images and satellite images

In this experiment, a small quadrotor (ENROUTE Co., Ltd., Fujimino, Japan), as shown in Figure 3, was used as the platform. Autonomous flights were conducted eight times at interval of about one week from winter wheat's heading stage to harvesting on June 2, 10, 19, 25, and July 2, 10, 16, 24, 2015 (at about 11:00 local time), using flight paths that were beforehand designed. Commercial camera SONY ILCE-6000 was used to take pictures in continuous mode every 2 s (f/8, 1/500 s, ISO 100). Flight altitude was set about 100 m above ground level, and during each flight camera was fixed upon a two-axis gimbal, pointing vertically downwards and took about 120 photos. Flight plan as well as camera specification was described in Table 1.

Eight orthomosaic images in total were made in Agisoft Photoscan Professional software (Agisoft LLC, Petersburg, Russia) by stitching about each 120 individual images together, respectively. Subsequently, georeferencing of orthomosaic images were accomplished using ArcMap 10.2 (Esri Inc., Redlands, Canada) software, which is the process of assigning geographic coordinates to data (usually an image file) that is spatial in nature but has no explicit geographic coordinates, for example aerial photographs. In this study, georeferencing was completed by using eight ground controlling points (GCP), which consist of headline corners, telegraph poles around the test field.

First order polynomial transformation creates two least-square-fit equations by comparing the image space coordinates of the GCPs with the geographic coordinates (latitude and longitude) and translates image coordinates of each pixel into geographic coordinates. These GCPs' geo-spatial coordinates were measured by using Trimble SPS855 GNSS modular receiver in RTK-GPS mode. And the result of orthomosaic image's georeferencing was shown in Figure 4 as geo-spatially overlaid upon a satellite image.

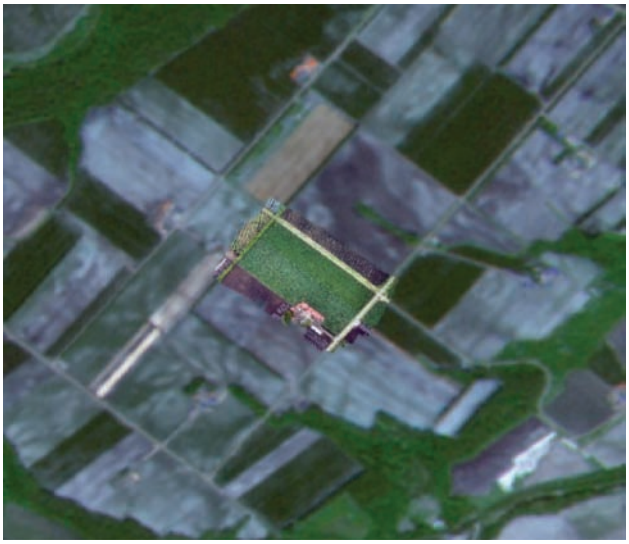

Figure 4 Geo-referenced UAV's image overlaid upon satellite image

Four ortho-rectified Rapideye satellite images were used in this study, the full scene size of which reach up to 3688×3687 pixels, and each satellite image covers about 550 km^2. Satellite images' details of the studied area were also shown in true color mode in Figure 4, using the image taken on June 15, 2015 as an example.

2.3 Radiometric normalization of multi-temporal remote sensing images

Due to varied atmospheric and different illumination conditions when reflectance data were recorded, radiometric accuracy and consistency are usually difficult to maintain among multi-temporal remote sensing images[22,23]. In this study, the relative radiometric correction, or radiometric normalization, was performed to adjust multi-temporal remote sensing images to a set of reference data by building linear regression models, band by band. The reference data were generated by calculating average values of each pseudo-invariant features' (PIF) pixel value from four satellite images and eight RGB images acquired from UAV, and PIF refers to the ground objects of which reflectance values are nearly constant over time during a certain period[24].

As to satellite remote sensing images, 38 crossroads and 2 flat grounds nearby construction sites, covering considerable large area around the experimental fields, were selected as PIFs by visual inspection, marked as dark dots shown in Figure 5. On the other hand, 7 places along road as well as 5 places on roof nearby the test fields were chosen as PIFs in each UAV's RGB images, and around each PIF mean values of 6 pixels distributed within 1 m^2 were calculated so that influences of abnormal values caused by foreign matters could be reduced. Spatial distribution of UAV's RGB images' PIFs is described as Figure 6. As a result, based on these linear-regression models between pixel values of each image's PIF and the reference dataset, each band of all images was normalized and effects caused by deviation of atmospheric or illuminative condition could be compensated so that real changes of crop canopy could be extracted in multi-temporal analysis.

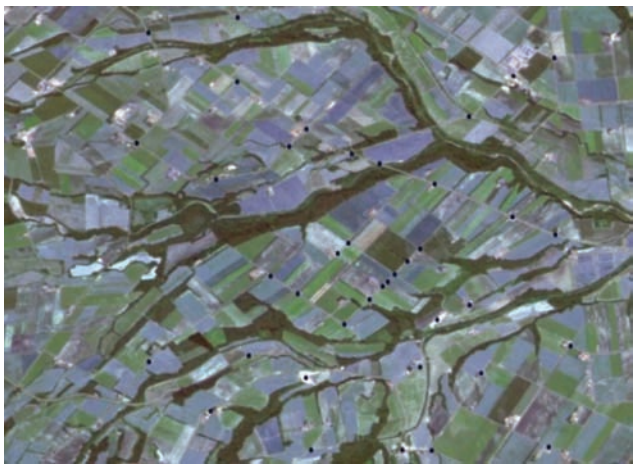

Figure 5 Spatial distribution of satellite images' PIFs

Figure 6 Spatial distribution of UAV's RGB images' PIFs

2.4 Sampling of grain protein contents

Twelve samples of field No.1 (Kitahonami) and eight samples of field No.2 (Yumechikara) were randomly taken after field survey to measure grain protein contents, and the samples' spatial distribution was shown on a UAV's RGB image in Figure 2. Sampling operation was conducted on July 24, 2015, two days ahead of harvesting, by collecting wheat ears within each specified 1-square-meter section. These samples' geo-coordinates were also acquired by using Trimble SPS855 GNSS modular receiver in RTK-GPS mode. After threshing and cleaning, grain protein contents were measured by using a near-infrared spectrometer BR-5000 of Shizuoka Seiki Co., Ltd[16], and results were recorded in Table 2.

Table 2 Geographical coordinates and grain protein contents of twenty wheat samples

	Sample ID	Longitude	Latitude	Protein content/%
Field No.1	1	142.978073	42.90145059	13.58
	2	142.9786421	42.90165733	12.96
	3	142.9792217	42.90130743	13.53
	4	142.9795698	42.9010971	12.00
	5	142.9804969	42.9005315	12.71
	6	142.9810695	42.90017927	12.78
	7	142.9813016	42.90035963	12.18
	8	142.9807589	42.90069382	12.13
	9	142.9802862	42.90097218	12.76
	10	142.979924	42.90120185	12.17
	11	142.9794719	42.90147593	12.60
	12	142.9788905	42.901832	12.67
Field No.2	13	142.9790211	42.90224562	15.46
	14	142.9791964	42.90214069	14.83
	15	142.9797338	42.90181557	14.30
	16	142.9800688	42.9016125	14.51
	17	142.980186	42.90154186	14.59
	18	142.9804643	42.90136493	14.27
	19	142.9809515	42.90107865	13.81
	20	142.9815535	42.90071446	13.54

2.5 Extracting vegetation indices from satellite images and UAV's RGB images

NDVI and VDVI are the most well-known and widely used vegetation indices to detect live plant canopies, and NDVI even could be used to quantify the photosynthetic conditions and vitalities as near-infrared band is highly sensitive to chlorophyll contents in live plants.

$$NDVI=(NIR-RED)/(NIR+RED) \quad (1)$$

where, "*NIR*", and "*RED*" is the radiometric normalized pixel values of near-infrared band and red band of satellite images, respectively.

$$VDVI=(2G-B-RED)/(2G+B+RED) \quad (2)$$

where, *G*, *B* and *RED* are the radiometric normalized pixel values of green band, blue band, and red band of satellite images as well as UAV's RGB images, respectively.

In this study, firstly twenty NDVI samples out of four satellite images were derived by using ENVI software (Exelis VIS, Inc., Colorado, US), respectively, at the same position with that of sampled grain protein contents (shown in Figure 2) by inputting geographical coordinates described in Table 2; subsequently, forty vegetation indices' samples (each twenty samples for field Kitahonami and Yumechikara, respectively) of NDVI as well as VDVI out of each satellite images were extracted, and at the same sampling positions corresponding forty samples of VDVI were calculated out of four UAV's images that are temporally nearby the acquisition date of satellite images for correlation analysis. Spatial distribution of forty vegetation indices samples is also described in a NDVI map based on satellite image taken on June 15, 2015 in Figure 7.

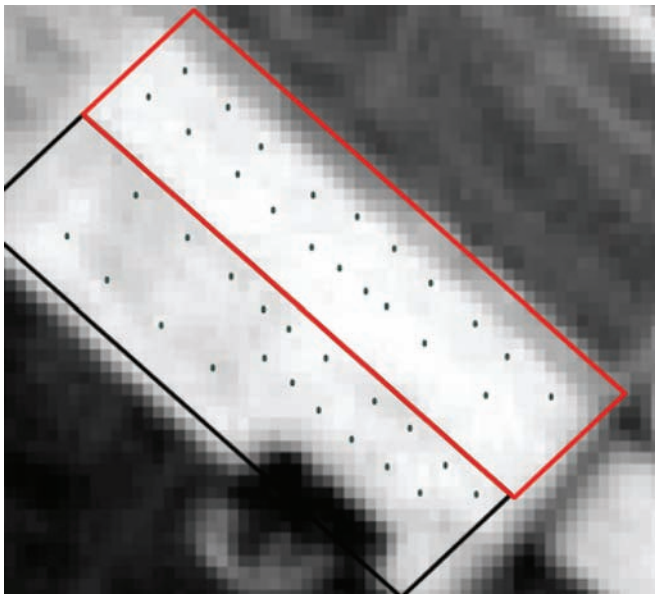

Figure 7 Spatial distribution of vegetation indices

3 Results and discussion

3.1 Visual inspection of wheat growth status from multi-temporal satellite and UAV's RGB images

From multi-temporal satellite images, shown in Figure 8 in both true color mode and Figure 9 in standard false color mode which is combined of near-infrared band, red band, and green band, we could get general

understanding of color change of wheat canopy. In true color mode, conclusions were reached that greenness of two wheat fields did not differ too much from each other, and kept increasing to the date of June 15, while began to decrease since then due to ripening process. Besides, within-field spatial variations of canopy density as well as greenness could not be clearly observed due to rather sparse spatial resolution of satellite images; however, abrupt brightness occurred around up-left corner of the last image taken on July 17 (spotted in red circle), which roughly showed the lodged wheat canopy's position in field No.1 of Kitahonami (marked in black line). Remote sensing images demonstrated in standard false color mode have widespread applications in vegetation detection, forest derivation, crop monitoring, etc., as live plants are featured to have strong reflectance in near-infrared band. Figure 9 shows the Rapideye satellite images in standard false color, from which within-field spatial variations of canopy color were clearly observed and occurrence of lodging were spotted around over-flourished areas (marked in yellow circle) in field No.1 marked in black box. On the contrary, filed No.2 showed rather homogeneous characteristics of canopy development, and no lodging happened throughout the field. Conclusion could also be reached that until June 15 both the two fields showed vigorous vegetative growth conditions, and since then no more bright-red areas were found in both two fields in the last image taken about 10 d prior to harvesting on July 17, which indicated the dying out process of wheat canopies.

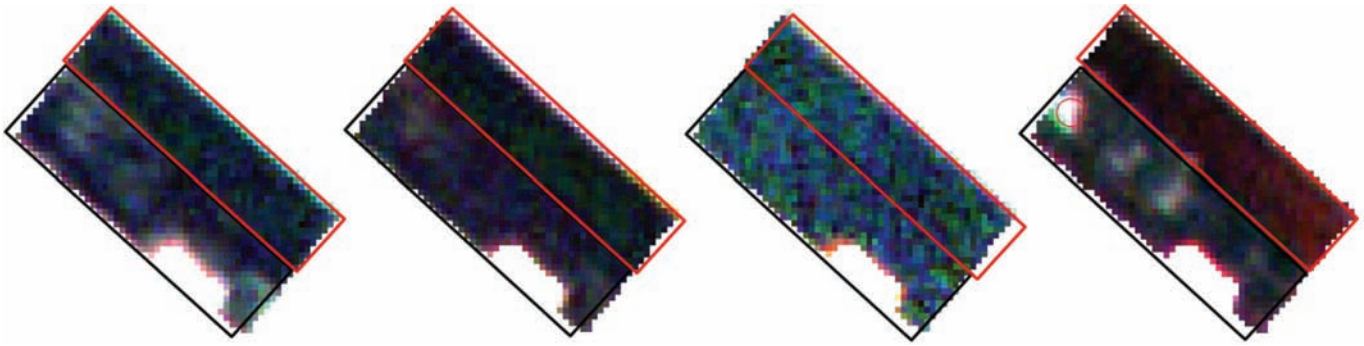

Figure 8 Color change of wheat canopy shown by using multi-temporal satellite images in true color mode (Images that were taken on June 1, 7, 15, and July 17, 2015 demonstrated in sequence from left to right)

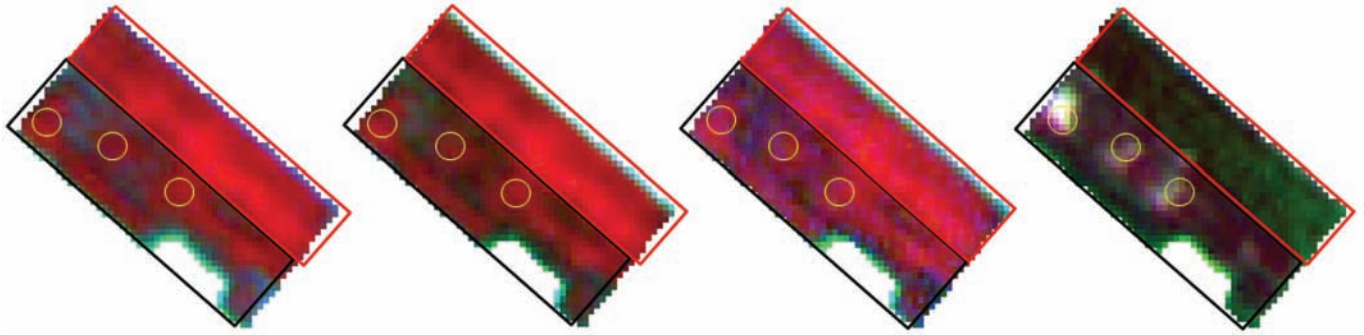

Figure 9 Color change of wheat canopy was showed by using multi-temporal satellite images in standard false color mode (Images that were taken on June 1, 7, 15, and July 17, 2015 demonstrated in sequence from left to right)

As temporal frequency of satellite images is not adequate for monitoring the rapid changing wheat growth status, another 8 UAV's RGB images were used as shown in Figure 10. From UAV's RGB images, straightforward visualization of real wheat growth status was acquired through visual interpretation that within-field variations of wheat canopy density are so obvious that existence of bare soil could be noticed from the image taken on June 2 when wheat canopy was in its early growth stages. In terms of time-domain, canopy greenness of both two wheat varieties reached peak value on June 10, 2015, and there is no significant difference of canopy greenness between these two different wheat varieties in early growth stages; however, from June 10, 2015 it became distinctive that field No.2 (marked in red box) showed heavier canopy greenness compared with

the other one. In image taken on June 2, 2015 of field No.1 (marked in black box) such areas marked in black circle had relatively higher level of stalk densities, and compounded with other environmental influences such as rainfall, wind, and etc., it eventually led to occurrence of lodging at growth stage of grain-filling when the over-luxuriant canopies failed to support heavy wheat ears, showed in image of July 16 and 24, 2015 where circled in black. Figure 11 showed a close-shot photograph of the lodging spot in field No.1, taken on July 16, 2015. It suggested that UAV's RGB image taken about one week ahead of harvesting could be practically served as navigation references which guide either drivers of combine harvesters, or autonomous harvesting vehicles, to adjust operation speed according to the specific lodging situations for less loss rate of harvesting, as occurrence of lodging in wheat field has been generally considered as the most influencing and direct factor which impairs the working performance of combine harvester.

Figure 10 UAV's RGB images of wheat fields from heading stage to harvesting (the upper four images from left to right were taken on June 2, 10, 19 and 25, and the lower four images from left to right were taken on July 2, 10, 16 and 24, 2015)

Figure 11 Close-shot photograph of the lodging spot in test wheat field, taken on July 16, 2015

3.2 Monitoring multi-temporal changes of vegetation indices derived from satellite images and UAV's RGB images

In order to further analyze time-varying crop canopy color changes, forty NDVI as well as VDVI samples were derived out of each satellite images, and at the same sampling positions corresponding forty samples of VDVI were calculated out of each UAV's RGB images. According to Table 3, the increasing trend of satellite image based NDVI as well as VDVI values was very clear at early growth stages, and then NDVI values began to decrease stage by stage to minimum value around 0.19, which is showed in Figure 12. On the other hand, VDVI values calculated from satellite images suggested the same tendency with the NDVI counterpart that VDVI reached maximum values on June 7 and then began to decrease as wheat changed from vegetative growth into reproductive process. Besides, big data variation of VDVI values derived from satellite images around wheat ripening stage may be a rather big issue when used for quantitative inversion with ground variables, as VDVI is

not as reliable as NDVI if crops are in the process of ripening or yellowing when VDVI values fall around the threshold value of 0, although VDVI is confirmed to be capable of differentiating and classifying vegetative areas from non-vegetative areas. Data on June 15 and July 17 indicated that most of VDVI values were found to be negative numbers, which could be due to the interference of soil pixels compounding with other reasons such as lodging.

Table 3 Time-varying NDVI and VDVI values of wheat fields calculated from satellite images

	Date	Average	Standard deviation
Satellite NDVI	June 1	0.54	0.04
	June 7e	0.72	0.04
	June 15	0.57	0.03
	July 17	0.19	0.05
Satellite NDVI	June 1	0.54	0.04
	June 7	0.72	0.04
	June 15	0.57	0.03
	July 17	0.19	0.05

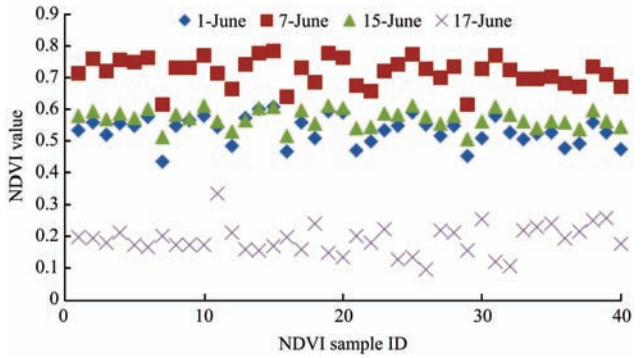

Figure 12 Time-varying NDVI values of wheat fields calculated from satellite images

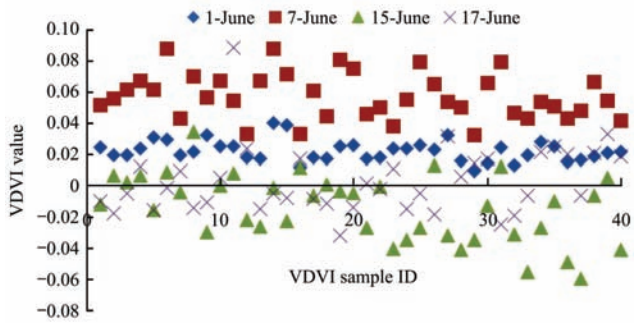

Figure 13 Time-varying VDVI values of wheat fields calculated from satellite images

To compare UAV's RGB image based VDVI with satellite image based VDVI as well as NDVI, a mean filter was firstly designed to average 39×39 pixel values of each VDVI map generated from UAV's RGB images, so that spatial resolution of UAV's RGB image based VDVI and satellite image based VDVI could be coordinated. From UAV's RGB images' time-varying VDVI data, conclusion was reached which is very alike with the one we made by observing multi-temporal changes of satellite image based NDVI as well as satellite image based VDVI. Firstly UAV's RGB image based VDVI values increased until June 10 and then began to decrease stage by stage to the minimum value around 0.02. The difference of UAV's RGB image based VDVI from satellite image based VDVI is that all UAV's RGB image based VDVI values were found to be positive numbers even until July 24, 2 d prior to harvesting, which once again confirmed VDVI's capability to differentiate vegetative areas from non-vegetative areas. The reason could be that fine ground resolution of UAV's RGB images eliminated soil interference.

Table 4 Time-varying VDVI values of wheat fields calculated from UAV's RGB images

	Date	Average	Standard deviation
UAV VDVI	June 2	0.12	0.01
	June 10	0.15	0.02
	June 19	0.08	0.03
	June 25	0.14	0.02
	July 2	0.10	0.02
	July 10	0.10	0.01
	July 16	0.06	0.01
	July 24	0.02	0.01

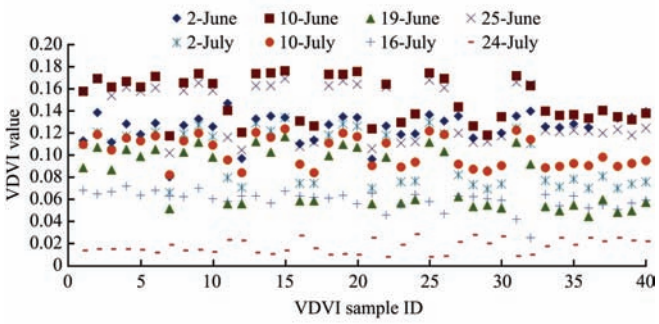

Figure 14 Time-varying VDVI values of wheat fields calculated from UAV's RGB images

3.3 Correlation analysis of satellite image based NDVI with grain protein contents

After extracting NDVI values from each satellite image at positions where grain protein contents were sampled showed in Figure 2, correlation coefficients of NDVI on different dates with the sampled grain protein contents were calculated in R software. As a result, correlation coefficients of grain protein content with

NDVI on June 1, 7, 15, and July 17 was calculated as 0.77, 0.79, 0.68, and -0.34, respectively. Conclusion could be reached that NDVI of satellite image have good correlation with grain protein contents before ripening growth stage around June 7, 2015, while the reliability of using satellite image based NDVI to predict grain protein contents becomes worse as ripening stage approaches. To further analyze relationship between NDVI and grain protein contents, different regression models such as linear, exponential, power, and second-order polynomial regressions were constructed by using NDVI data on June 7, respectively, on which date NDVI has the highest correlation coefficient with grain protein contents. From Figure 15 we can see that coefficient of determination values of these four different regression model do not vary too much from each other, while second-order polynomial regression model fitted the regression model best between satellite images based NDVI and sampled grain protein contents, with the coefficient of determination value of 0.67 and RMSE of 0.58.

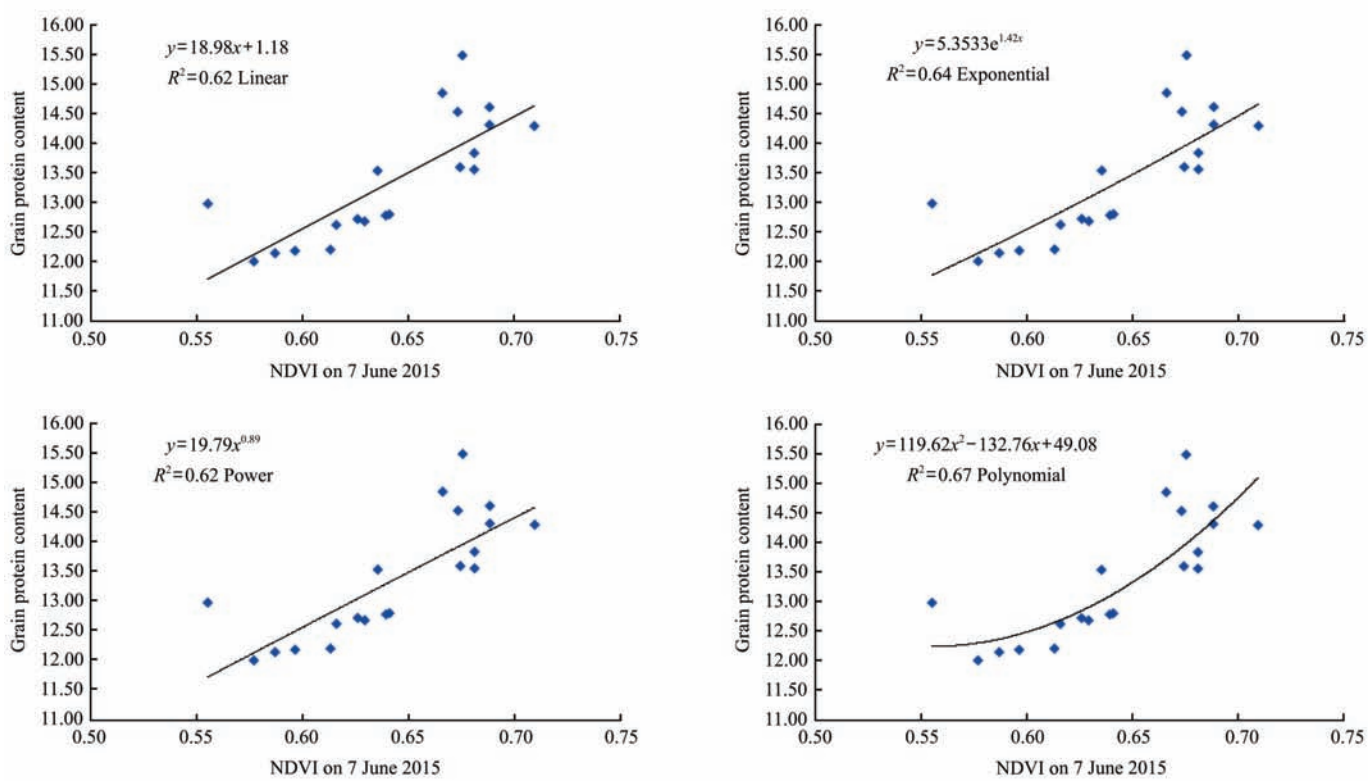

Figure 15 Linear, exponential, power, and second-order polynomial regression model of satellite image based NDVI on 7 June 2015 with sampled grain protein contents

3.4 Correlation analysis of vegetation indices of satellite images with UAV's RGB images

Correlation analysis of vegetation indices based on satellite images and UAV's RGB images was tentatively performed by building regression models. All of four satellite images and four out of eight UAV's RGB images that were taken temporally around the dates of satellite images were used, from which 40 training samples of UAV's RGB image based VDVI and 40 satellite images based NDVI samples as well as VDVI samples were extracted, respectively. And mean filter of 39×39 kernels was applied to UAV's RGB image based VDVI maps so that noise signal of bare soil could be reduced and spatial resolution of UAV's RGB image based VDVI map and satellite image based NDVI map as well satellite image based VDVI map could be coordinated. Regression analysis showed that second-order polynomial models fitted best between UAV's RGB image based VDVI and satellite image based VDVI as well as satellite image based NDVI, when compared with other regression models such as linear, exponential, and power. Coefficient of determination and RMSE are calculated as 0.62 and 0.019 for second-order polynomial regression model between UAV's RGB image based VDVI and satellite image based VDVI, while 0.58 and 0.127 for second-order polynomial regression model between

UAV's RGB image based VDVI and satellite image based NDVI, respectively. From Figure 16 conclusion was reached that at later stage of wheat growth season values of UAV's RGB image based VDVI decreased rapidly to around 0.05, and showed little correlation with the corresponding satellite image based VDVI values, which scattered from –0.06 to 0.1. Reasons could be that sparse ground resolution of satellite images inevitably led to less accurate minus VDVI values, as crops are dying out and non-vegetative pixels become predominant, making satellite image based VDVI values less reliable. On the other hand, Figure 17 indicated that satellite image based NDVI has better performance to reflect within-field spatial variations of wheat growth status at ripening or yellowing growth stages, as NDVI included near-infrared band which is reported to be sensitive and corresponsive to live vegetation. Therefore, high correlations between UAV's RGB image based VDVI and satellite image based VDVI as well as NDVI indicate that it is feasible and practical to temporally complement satellite remote sensing by using UAV's RGB images based vegetation indices to monitor wheat growth status.

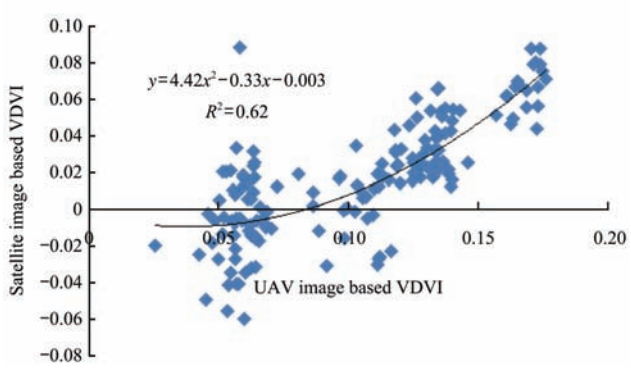

Figure 16 Second-order polynomial regression model between UAV's RGB images based VDVI and satellite images based VDVI

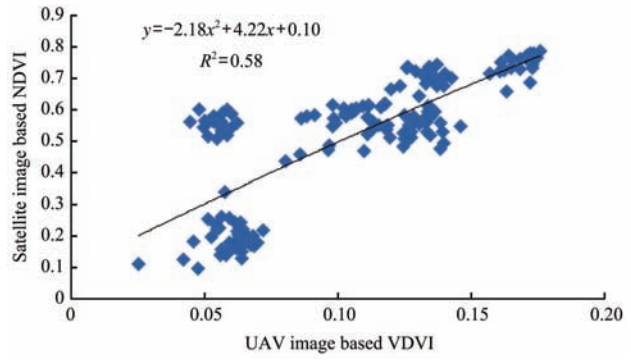

Figure 17 Second-order polynomial regression models of UAV's RGB images based VDVI and satellite images based NDVI

4 Discussions

Civilian use of UAVs opens up a new way of obtaining field information at farmland level. However, since UAV altitude directly affects image spatial resolution and image quality, which in turn changes vegetation indices' value by weakening or strengthening background (soil or crop residues) interferences, appropriate flight plan and specific processing of vegetation indices should be taken into consideration when conducting quantitative analysis. In this study, we built different regression models between satellite images based NDVI and sampled grain protein contents, and between satellite images based NDVI as well as VDVI and UAV's RGB image based VDVI. All regression models showed good or moderate coefficients of determination; however, it should be noted that timing as well as weather condition of UAV's RGB image acquisition matter a lot, and accordingly multi-temporal UAV's RGB image acquisition is highly recommended for quantitative inversion related studies, instead of one-time operation. Correlation analysis results in this study showed scientific and theoretical basis for promoting civilian UAV applications in agricultural industry.

5 Conclusions

Multi-temporal UAV's RGB images demonstrated high performance to intuitively monitor wheat canopy color change and to spot occurrence of lodging through visual inspection, while lodging has been widely considered as the main cause of deteriorating of grain quality and high loss rate of harvesting. Within-field spatial variations of canopy density as well as canopy color showed in UAV's RGB images taken at the early stage of wheat growth suggested that UAV's RGB images could be used as prescription for variable-rate fertilizing, as variable-rate fertilizing properly decreases the use of fertilizer upon over-luxuriant areas to prevent, or alleviate, the occurrence of wheat lodging. Besides, UAV's RGB images taken about one week ahead of harvesting could also be practically served as navigation references to guide either drivers of combine harvesters

or autonomous harvesting vehicles, to adjust operation speed according to the specific lodging situations for less loss rate of harvesting, as occurrence of lodging in wheat field has been generally considered as the most influencing and direct factor which impairs the working performance of combine harvester.

Through monitoring changes of both satellite image based NDVI as well as VDVI values and UAV's RGB image based VDVI values, conclusion was reached that all of these three vegetation indices have the same and synchronized trend of increasing at first, reaching up to peak values around June 7-10, 2015 before wheat's reproductive growth begins, and starting to decrease since then. By observing the time-varying values of vegetation indices, conclusions could also be reached that UAV's RGB images with fine spatial resolution demonstrated good performance because pixel values are less affected by background interference when compared with satellite images, and that it could be feasible of using commercial camera which is mounted upon small UAVs to conduct both qualitative and quantitative study on crop monitoring.

According to the results of the correlation analysis between satellite image based NDVI with sampled grain protein contents, NDVI of satellite images taken on June 1, 7, 15, and July 17, 2015 correlated with the sampled grain protein contents with the correlation coefficients being calculated as 0.77, 0.79, 0.68, and –0.34, respectively. Conclusions could be made that NDVI has good predicative capability for mapping grain protein content before ripening growth stage around June 7, 2015, while the reliability of using satellite image based NDVI to predict grain protein contents becomes worse as ripening stage approaches.

Correlation analysis of vegetation indices based on satellite images and UAV's RGB images was tentatively performed by building regression models. And the regression analysis between UAV's RGB image based VDVI and satellite image based VDVI as well as NDVI showed good coefficients of determination. Therefore, we conclude that it is feasible and practical to temporally complement satellite remote sensing by using UAV's RGB images based color vegetation indices to monitor wheat growth status and to map the within-field spatial variations of grain protein contents, in case that satellite images are not available or cost-effective for small scale farmlands .

Acknowledgement

This study was supported by the R&D Program of Fundamental Technology and Utilization of Social Big Data by the National Institute of Information and Communications Technology (NICT), Japan.

[References]

[1] Zadoks J C, Chang T T, Konzak C F. A decimal code for the growth stages of cereals. Weed Res., 1974: 14: 415–421.

[2] Poole N. Cereal growth stages, Grains research & development corporation, Lincoln, New Zealand, FAR, 2005.

[3] Weisz R. Small grain production guide revised March 2013, http://www.smallgrains.ncsu.edu/production-guide.html. Accessed on [2016-12-01].

[4] Rouse J W, Haas R H, Schell J A, Deering D W. Monitoring vegetation systems in the Great Plains with ERTS, Third ERTS Symposium, NASA SP-351 I, 1973; pp.309–317.

[5] Benedetti R, Rossini P. On the use of NDVI profiles as a tool for agricultural statistics: The case study of wheat yield estimate and forecast in Emilia Romagna. Remote Sensing of Environment, 1993; 45(3): 311–326.

[6] Mulla D J. Twenty five years of remote sensing in precision agriculture: Key advances and remaining knowledge gaps. Biosystems Engineering, 2013; 114: 358–371.

[7] Satellite image corporation, RapidEye Satellite Sensor. http://www.satimagingcorp.com/satellite-sensors/other-satellite-sensors/rapideye/. Accessed on [2016-12-05]

[8] Chander G, Haque M O, Sampath A, Brunn A, Trosset G, Hoffmann D, et al. Radiometric and geometric assessment of data from the RapidEye constellation of satellites, International Journal of Remote Sensing, 2013; 34(16): 5905–5925.

[9] Colewell R N. Determining the prevalence of certain cereal crop diseases by means of aerial photography. Hilgardia, 1956; 26: 223–286.

[10] Trout T J, Johnson L F, Gartung J. Remote sensing of canopy cover in horticultural crops. Hort. Science, 2008; 43(2): 333–337.

[11] Eisenbeiss H. A mini unmanned aerial vehicle (UAV): System overview and image acquisition. Image Acquisiton International Workshop on Processing and Visualization using High-Resolution Imagery, Pitsanulok, Thailand, 2004.

[12] Du M M, Noguchi N. Monitoring of wheat growth status and mapping of wheat yield's within-field spatial variations using color images acquired from UAV-camera system. Remote Sensing, 2017; 9(3): 289.

[13] Campbell J B, Wynne R H. Introduction to remote sensing. 5th edition. The Guilford Press, New York, USA, 2011; pp.72–102.

[14] Wang X Q, Wang M M, Wang S Q, Wu Y D. Extraction of vegetation information from visible unmanned aerial vehicle images. Transactions of the CSAE, 2015; 31(5): 152–159.

[15] Hunt E R, Hively J W D, Fujikawa S J, Linden D S, Daughtry C S T, McCarty G W. Acquisition of NIR-green-blue digital photographs from unmanned aircraft for crop monitoring. Remote Sens, 2010; 2: 290–305.

[16] Torres-Sánchez J, López-Granados F, de Castro A I, Peña-Barragán J M. Configuration and specifications of an unmanned aerial vehicle (UAV) for early site specific weed management. PLoS One, 2013; 8(3): e58210.

[17] Gamon J A, Surfus J S. Assessing leaf pigment content and activity with a reflectometer. New Phytologist, 1999; 143(1): 105–117.

[18] Woebbecke D M, Meyer G E, Von Bargen K, Mortensen D A. Color indices for weed identification under various soil, residue and lighting conditions. Transactions of the ASAE 1995; 38(1): 259–269.

[19] Rasmussen J, Ntakos G, Nielsen J, Svensgaard J, Poulsen R N, Christensen S. Are vegetation indices derived from consumer-grade cameras mounted on UAVs sufficiently reliable for assessing experimental plots? European Journal of Agronomy, 2016; 74: 75–92.

[20] http://www.data.jma.go.jp/obd/stats/etrn/view/annually_a.php?prec_no=20&block_no=0115&year=2015&month=&day=&view=p1. Accessed on [2017-05-20]

[21] MAFF. http://www.maff.go.jp/. Accessed on [2016-11-10]

[22] Vermote E F, Tanre D, Deuze J L, Herman M, Morcrette J J. Second simulation of the satellite signal in the solar spectrum, 6S: An overview. IEEE T. Geosci. Remote, 1997; 35: 675–686.

[23] Berk A, Bernstein L, Robertson D. MODTRAN: a moderate resolution model for LOWTRAN7, Tech. Rep. GL-TR-89-0122, Air Force Geophysics Lab, Hanscom AFB, Massachusetts, USA, 1989.

[24] de Carvalho Júnior O A, Guimarães R F, Silva N C, Gillespie A R, Gomes R A T, Silva C R, et al. Radiometric normalization of temporal images combining automatic detection of pseudo-invariant features from the distance and similarity spectral measures, density scatterplot analysis, and robust regression. Remote Sens., 2013; 5: 2763–2794.